Billakurthi and Hibberd *Plant Methods* (2023) 19:69
https://doi.org/10.1186/s13007-023-01041-x

Plant Methods

METHODOLOGY Open Access

A rapid and robust leaf ablation method to visualize bundle sheath cells and chloroplasts in C_3 and C_4 grasses

Kumari Billakurthi[1*] and Julian M. Hibberd[1]

Abstract

Background It has been proposed that engineering the C_4 photosynthetic pathway into C_3 crops could significantly increase yield. This goal requires an increase in the chloroplast compartment of bundle sheath cells in C_3 species. To facilitate large-scale testing of candidate regulators of chloroplast development in the rice bundle sheath, a simple and robust method to phenotype this tissue in C_3 species is required.

Results We established a leaf ablation method to accelerate phenotyping of rice bundle sheath cells. The bundle sheath cells and chloroplasts were visualized using light and confocal laser microscopy. Bundle sheath cell dimensions, chloroplast area and chloroplast number per cell were measured from the images obtained by confocal laser microscopy. Bundle sheath cell dimensions of maize were also measured and compared with rice. Our data show that bundle sheath width but not length significantly differed between C_3 rice and C_4 maize. Comparison of paradermal versus transverse bundle sheath cell width indicated that bundle sheath cells were intact after leaf ablation. Moreover, comparisons of planar chloroplast areas and chloroplast numbers per bundle sheath cell between wild-type and transgenic rice lines expressing the maize *GOLDEN-2* (*ZmG2*) showed that the leaf ablation method allowed differences in chloroplast parameters to be detected.

Conclusions Leaf ablation is a simple approach to accessing bundle sheath cell files in C_3 species. We show that this method is suitable for obtaining parameters associated with bundle sheath cell size, chloroplast area and chloroplast number per cell.

Keywords *Oryza sativa*, Leaf ablation, Bundle sheath cells, Chloroplasts, Confocal microscopy

*Correspondence:
Kumari Billakurthi
kb720@cam.ac.uk
[1]Department of Plant Sciences, University of Cambridge, Downing Street, Cambridge, UK

Background

Photosynthesis is fundamental to life on earth and allows assimilation of atmospheric CO_2 into biomass via the Calvin-Benson-Bassham or C_3 cycle [1–3]. In plants the photosynthetic process is broadly categorised into C_3, C_4 and Crassulacean Acid Metabolism based on the pathway of carbon fixation. However, plants that use C_3 photosynthesis predominate such that species using C_4 and Crassulacean Acid Metabolism account for only three and six% of land plants respectively [4–6]. In C_3 plants, mesophyll cells are filled with chloroplasts and so are the major site of photosynthesis (Fig. 1a). In these plants the enzyme Ribulose-1,5-Bisphosphate Carboxylase/Oxygenase (RuBisCO) carboxylates the five-carbon compound Ribulose-1,5-bisphosphate (RubP) via the C_3 cycle to generate two molecules of the three-carbon compound 3-phosphoglycerate. In contrast, in the vast majority of C_4 plants the reactions of carbon assimilation are equally partitioned between mesophyll and bundle sheath cells. HCO_3^{-1} is initially fixed in mesophyll cells by Phospho*enol*pyruvate Carboxylase (PEPC) to generate four-carbon compounds such as malate and aspartate that then diffuse into bundle sheath cells. Decarboxylation of either aspartate or malate in the bundle sheath releases high concentrations of CO_2 in bundle sheath cells that can then be assimilated by RuBisCO [7].

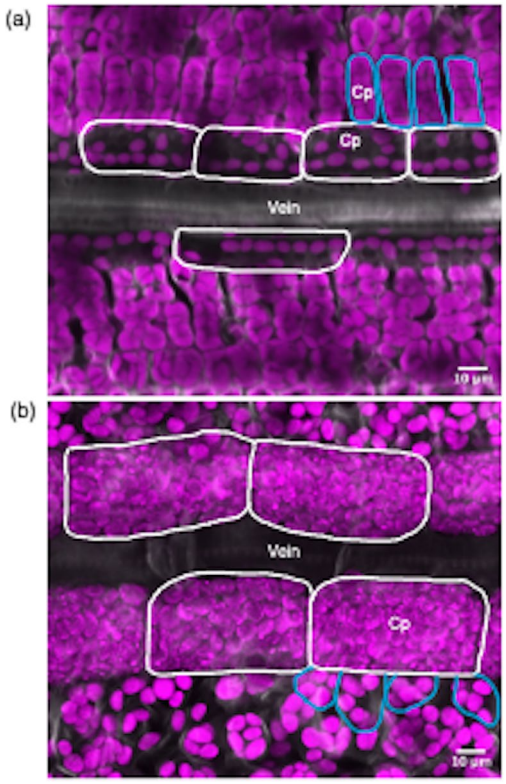

Fig. 1 Confocal laser scanning microscopy images of C_3 (rice) and C_4 (maize) mesophyll and bundle sheath cells. Images are derived from paradermal sections. Representative maximum intensity projection image of a Z-stack from wild type rice (**a**) and maize (**b**). Bundle sheath and mesophyll cells are highlighted with white and blue lines respectively. Chloroplasts from bundle sheath cells of maize generate lower autofluorescence due to lower amounts of Photosystem II. Cp: Chloroplasts (pseudo colour: magenta)

Due to the C_4 cycle concentrating CO_2 around RuBisCO, C_4 species are more efficient under dry and high-temperature conditions. Moreover, they often have improved water and nitrogen use efficiencies compared with C_3 plants [8–11]. Apart from those species that use single-celled C_4 photosynthesis [12], a unifying character underpinning the C_4 pathway is a specialised form of leaf morphology termed Kranz anatomy [13]. Kranz anatomy is characterised by a high vein density and bundle sheath cells that are altered both morphologically but also in terms of organelle occupancy and positioning. During the C_3 to C_4 trajectory, in some lineages while not always the case, evolution has generated bundle sheath cells that are larger in the medio-lateral leaf axis [14, 15] and contain numerous larger chloroplasts ([16], Fig. 1b).

Increasing the photosynthetic efficiency of C_3 crops would help meet future demands for food, especially under changing climatic conditions. It has been predicted that introducing the C_4 pathway into C_3 crops could increase their photosynthetic efficiency by up to 50% [17]. However, one of the main bottlenecks is an incomplete understanding of how bundle sheath cells become photosynthetically activated in C_4 plants. On average, the bundle sheath chloroplast content of C_4 species is ~30% more than in C_3 species [16, 18], but how this evolved is not fully understood. The GOLDEN2-LIKE family of transcription factors known to regulate chloroplast development in C_4 species [19–21]. Although overexpression of *GOLDEN2* or *GOLDEN2-LIKE 1* from C_4*Zea mays* in rice increased bundle sheath chloroplast volume, this did not phenocopy the increase in chloroplast occupancy found in C_4 plants [22].

Introducing C_4 bundle sheath anatomy into C_3 rice is therefore likely to involve large-scale testing of candidate genes involved in bundle sheath cell and chloroplast development and phenotyping bundle sheath cells. However, the bundle sheath has been challenging to phenotype in C_3 plants. Classical bright-field light microscopy after embedding samples in resin and thin sectioning has been used [18]. Although this is simple and easily available, it only captures two-dimensional (2D) information from a thin section. 2D-transmission electron microscopy (2D-TEM) is widely used for characterising the ultracellular structure and organisation in photosynthetic cell types [23] but it is expensive and has the same limitations as light microscopy when cell and chloroplast parameters are being quantified. A single-cell isolation method has been established to study mesophyll and bundle-sheath cell dimensions and chloroplast

occupancy, but it requires enzymatic digestion of leaf tissue that might disturb cell integrity and chloroplast size [22]. Mechanical isolation of bundle sheath strands has previously been used for C_4 grasses [24, 25]. But, a number of chemical treatments are involved, and success depends on the correct preparation of leaf tissue as well as optimisation of the grinding procedure. Moreover, vein positional information is typically lost meaning that it is challenging to define the origin of bundle sheath cells. Furthermore, application of this method to C_3 grasses might not be feasible due to many mesophyll layers. Lastly, more advanced electron microscopy-based 3D reconstruction methods such as serial block-face scanning electron microscopy (SBF-SEM) can cover large fields of view and reconstruct ultrastructural features in 3D such that volume of leaf cells and chloroplasts can be quantified [26]. However, it is costly and labour-intensive. Thus, each of these approaches has disadvantages for high-throughput screening of bundle sheath cells in species such as C_3 rice.

To address this, we established a simple and robust method to expose bundle sheath cell files in rice and measure their cell dimensions, as well as the planar chloroplast area and chloroplast number per cell. We show that these bundle sheath cells are intact and the chloroplast number per cell is comparable with previous reports [22]. We also applied this method to the C_4 species maize to measure bundle sheath cell dimensions and made comparisons between bundle sheath cells in these two species. When combined with genetic perturbations we anticipate that this approach will provide insight into structure function relations of bundle sheath cells in species such as rice.

Results

A simple and robust method to visualize bundle sheath cells in C_3 rice and C_4 maize

The middle region of fully expanded fourth leaves from rice and maize was fixed with glutaraldehyde. Prior to ablation, although parallel venation was detectable in rice at low magnification, when higher power objectives were used the significant amount of light scattering meant that individual cells including the bundle sheath were not visible (Fig. 2a, c). However, bundle sheath strands and cells became visible (Fig. 2b, d) after the adaxial side of leaves was ablated by gentle scraping (Additional file 1). In rice scraping was carried out until mesophyll tissue surrounding intermediate veins appeared less green. As the bundle sheath is deep in the C_3 leaf because of the many layers of mesophyll cells [27], two to three minutes of ablation (Additional file 1) was required to expose bundle sheath cells around intermediate veins (Fig. 2b, d). Consistent with rice leaf anatomy, three to four intermediate veins (rank-1; tertiary; 3°) were present between the larger lateral (secondary; 2°) veins.

In maize, dark green strands that represent the bundle sheath were visible prior to scraping (Fig. 2e) and although mesophyll cells were detectable at higher magnification this was not true for the bundle sheath (Fig. 2g). Scraping of maize allowed files of dark green bundle sheath and the less green mesophyll cells to be identified (Fig. 2f). C_4 maize has increased numbers of intermediate (rank-1+rank-2) veins between the larger laterals because of an increase in the density of rank-2 intermediates [28] and leaf ablation was consistent with this (Fig. 2f). In C_4 maize it took less than one minute to ablate mesophyll layers such that bundle sheath cell files were clearly visible (Fig. 2f, h).

Quantification of bundle sheath cell dimensions

To provide quantitative insight into differences between bundle sheath cells of C_3 rice and C_4 maize we ablated leaf tissue from each species and then used calcofluor white to mark cell walls (Fig. 3a, b). Bundle sheath cell length and width measurements were taken at the midpoint of both the proximal-distal and medio-lateral axes, and planar cell area was calculated (Fig. 3a, b). Average bundle sheath cell width was 15 µm in rice and 32 µm in maize (Fig. 3c) but there is a very small difference in bundle sheath cell length between these two species (Fig. 3d). However, as a consequence of the increased width of bundle sheath cells in maize, mean bundle sheath cell area was significantly higher (1404 μm^2) than that of rice (598 μm^2) (Fig. 3e). We also observed high variance in bundle sheath cell dimensions in both rice and maize. This variation in width and length of bundle sheath cells was two-fold and three-fold respectively in both species (Fig. 3c, d), and the variation in bundle sheath cell area of maize was around 1.4 times greater than that of rice (Fig. 3e).

Visualisation and quantification of chloroplast parameters in rice bundle sheath cells

We next wished to investigate whether bundle sheath chloroplast number and size could be determined after leaf ablation. Transgenic rice lines expressing the maize *GOLDEN2* (*ZmG2*) transcription factor under the control of the maize ubiquitin promoter are known to contain larger chloroplasts [22] and so were used as controls. We used calcofluor white to stain cell walls and chlorophyll autofluorescence to visualize bundle sheath cell chloroplasts. Z-stacks of 82 and 90 bundle sheath cells from wild-type and p*ZmUbi*::*ZmG2* rice respectively were acquired by confocal laser scanning microscopy. Maximum intensity projection images (Fig. 4a) were used to quantify individual chloroplast areas and chloroplast number per cells. The average planar area of individual

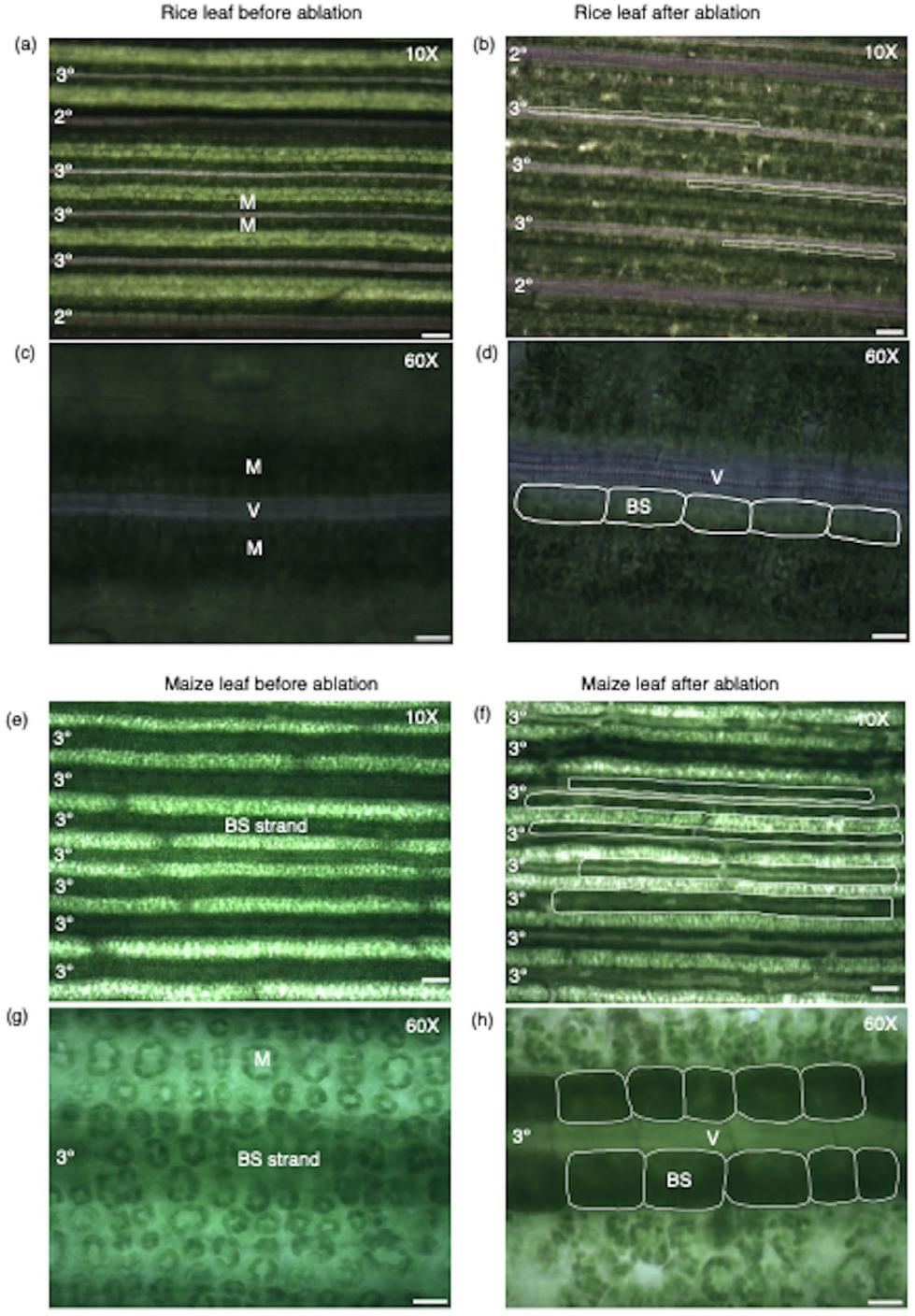

Fig. 2 Visualization of rice and maize leaves before and after ablation. Light microscopy images of rice (**a**–**d**) and maize (**e**–**h**) leaves before (left) and after scraping (right). Low power images (**b**, **f**) illustrating the impact of ablation on bundle sheath visibility (highlighted with white lines). Representative images of selected regions at higher magnification (**d**, **h**). Bundle sheath cells highlighted with white lines. Abbreviations are as follows: 2°: secondary veins; 3°: tertiary veins; V: Vein; BS: Bundle sheath cell. M: Mesophyll tissue. Scale bar represents 100 µm (**a**, **b**, **e**, **f**) and 20 µm (**c**, **d**, **g**, **h**)

bundle sheath chloroplasts in wild-type was ~17 µm^2 (with a range from 7 to 37 µm^2; Fig. 4b). Consistent with published data [22] planar area of bundle sheath chloroplasts was significantly increased in the p*ZmUbi*::*ZmG2* line and ranged from 7 to 54 µm^2 (Fig. 4b). Moreover, as expected [22] there was no difference in chloroplast numbers in the bundle sheath between controls and p*ZmUbi*::*ZmG2* (Fig. 4c). However, total chloroplast occupancy of bundle sheath cells in p*ZmUbi*::*ZmG2* was significantly increased due to the greater planar area of

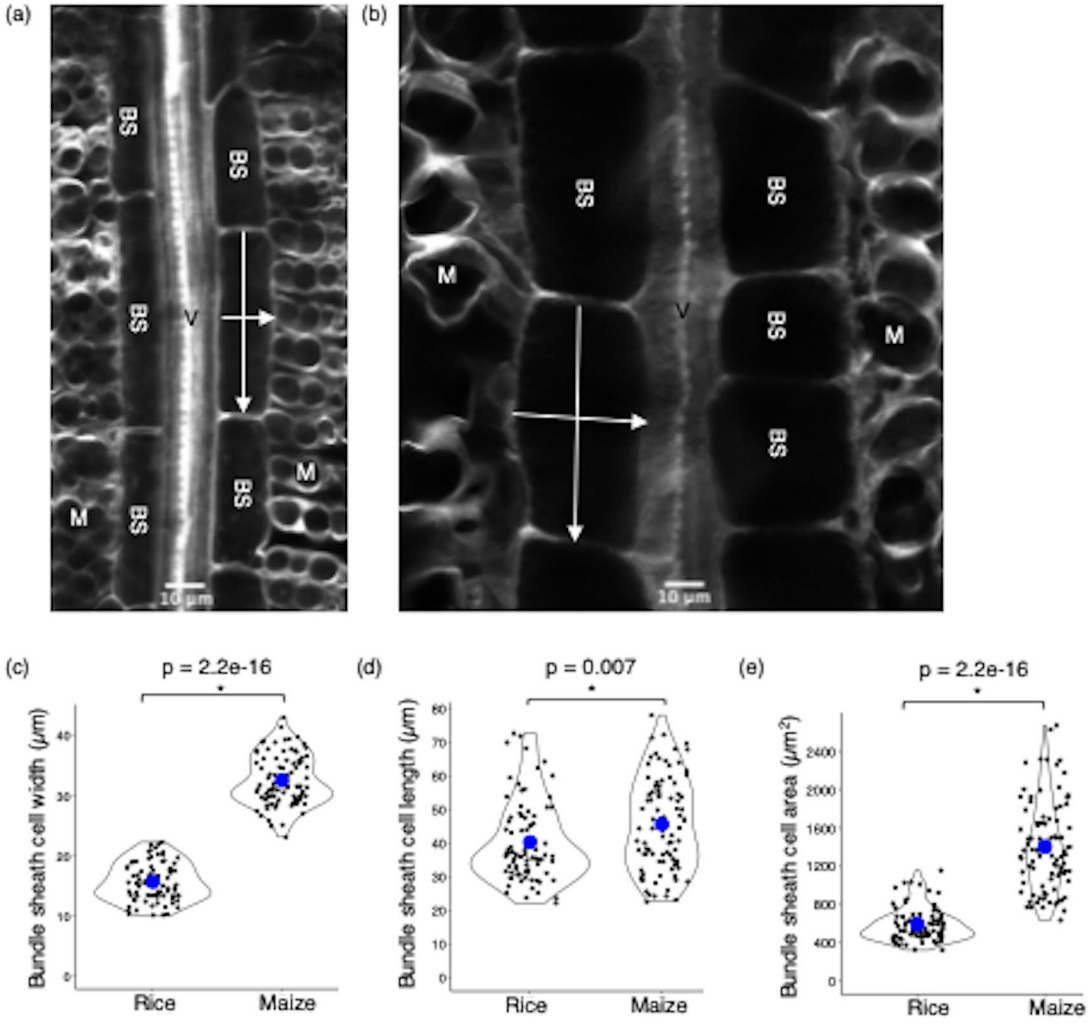

Fig. 3 Quantification of bundle sheath cell dimensions in rice and maize. **a** Representative confocal laser scanning microscopy images of calcofluor white stained (pseudo colour: grey) bundle sheath strand and mesophyll tissue of rice (**a**) or maize (**b**). Images were cropped to focus on a bundle sheath strand. Violin plots representing bundle sheath cell cell width (**c**), length (**d**) and area (**e**) in rice and maize. Blue dot represents mean values. Bundle sheath cell length and width measurements were taken at the mid-point of the proximal-distal and medio-lateral axes respectively (annotated with white arrows in a and b). Each observation represents one cell. Number of cells (n) = 82 and 90 from rice and maize, respectively. Abbreviations are as follows: V: Vein; BS: Bundle sheath cell; M: Mesophyll cell. Statistical test: t-test

individual chloroplasts (Fig. 4d). Further, total chloroplast number per bundle sheath cell (with a range from 8 to 25) obtained from leaf ablation (Fig. 4c) was comparable with that previously reported from analysis of isolated single-cells (with a range from 6 to 21; [22]). Therefore, gentle and careful ablation can be used to obtain accurate estimates of chloroplast numbers in rice bundle sheath cells.

Acquisition of three-dimensional (3D) images is of course more time consuming than two-dimensional (2D) images. We therefore wanted to test if there was a difference between bundle sheath chloroplast numbers estimated by the two approaches and so obtained 2D and 3D images of the same 31 cells from wild-type (Fig. 5a). These data showed that the bundle sheath chloroplast number was significantly higher (Fig. 5b) when estimated from 3D imaging (with a range from 11 to 25) compared with 2D imaging (with a range from 10 to 19). However, planar area of individual chloroplasts in bundle sheath cells was not different between the two datasets (Fig. 5c). We conclude that 3D imaging provides a more precise estimate of bundle sheath chloroplast numbers but either method can be used to quantify chloroplast size.

The relationship between bundle sheath paradermal cell area and chloroplasts

We wanted to use the above data to understand the relationship between bundle sheath chloroplast occupancy and cell area in rice. Therefore, a simple linear regression model was performed between bundle sheath paradermal

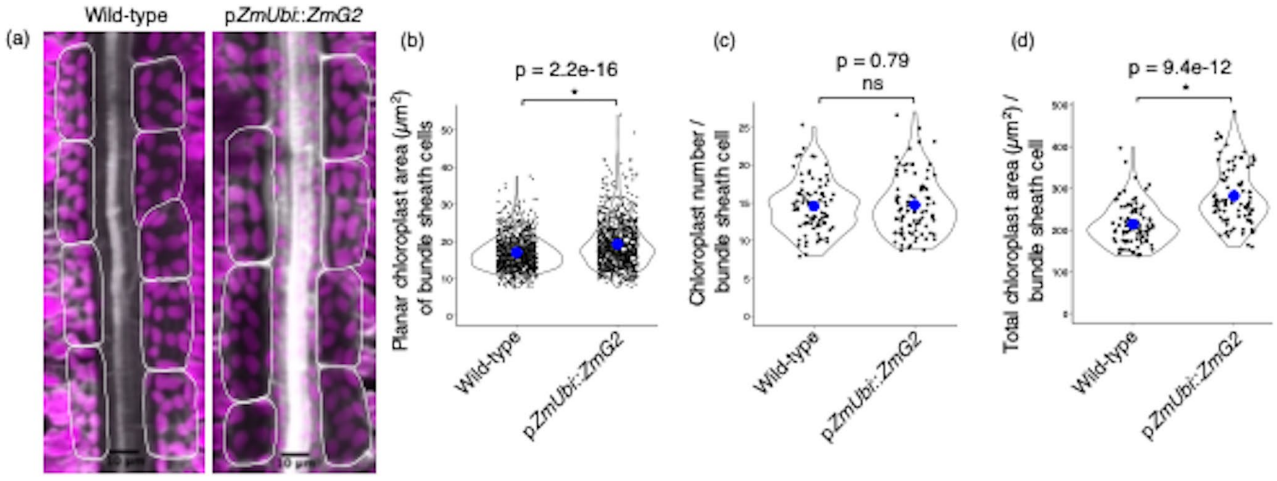

Fig. 4 Visualization and quantification of chloroplast area and number in the bundle sheath of rice. **a** Representative maximum intensity projection image of a Z-stack from wild-type and the *GOLDEN2* overexpressing line (p*ZmUbi*::*ZmG2*). Images were cropped to focus on a bundle sheath strand. Bundle sheath cells are highlighted with white lines. **b** Planar area of individual chloroplasts from bundle sheath cells. Each observation represents one chloroplast. Number of chloroplasts (n) = 1032 and 1114 from wild-type and p*ZmUbi*::*ZmG2* rice lines, respectively. **c** Chloroplast number per bundle sheath cell. Each observation represents one cell. **d** Total chloroplast area per bundle sheath cell. Each observation represents the total chloroplast area of a cell. Number of cells (n) = 82 and 90 from wild-type and p*ZmUbi*::*ZmG2* rice lines, respectively. Blue dot in the violin plots represent mean values. Statistical test: t-test

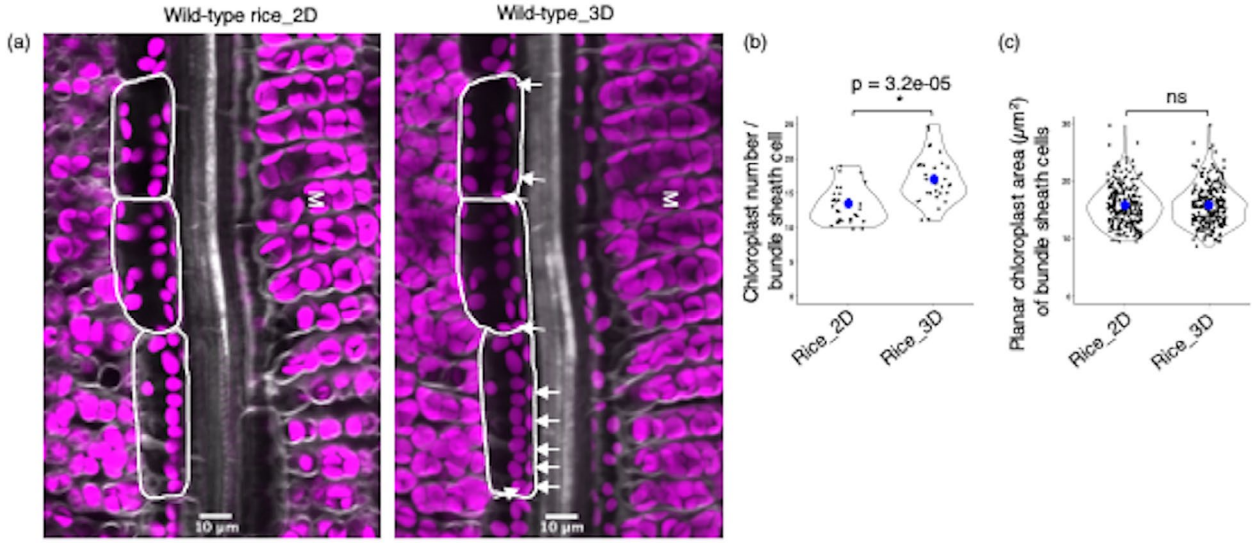

Fig. 5 Comparison of chloroplast numbers obtained from two and three-dimensional (2D and 3D) imaging. **a** Representative two-dimensional (left) and three-dimensional (right) images of wild-type rice leaves. Bundle sheath cells are highlighted with white lines. Chloroplasts present in the 3D image but not detected in the 2D image are highlighted with white arrows. **b** Chloroplast number per bundle sheath cell - each observation represents one cell (n = 31). **c** Planar chloroplast area of bundle sheath cells - each observation represents one chloroplast. Number of chloroplasts (n) = 236 and 242 from 2D and 3D imaging, respectively. Blue dot in the violin plots represent mean values. Statistical test: t-test. M: Mesophyll tissue

cell area and chloroplast size and number. This showed that the average planar and maximum chloroplast area per cell did not vary with bundle sheath cell area (Fig. 6a, b). But, chloroplast number and thus total chloroplast area per cell increased with cell area (Fig. 6c and d). The percentage of cell area occupied by chloroplasts was negatively correlated with bundle sheath cell area (Fig. 6e).

Discussion

It is widely recognised that improving photosynthesis in crops is one mechanism to improve yield [29]. One approach that has been proposed [17, 30] is to engineer the C_4 pathway into C_3 crops such as rice and it is estimated that this could improve yields by up to 50%. However, this goal is challenging and would require a significant increase in the chloroplast compartment of bundle sheath cells from C_3 crops such as rice. It has

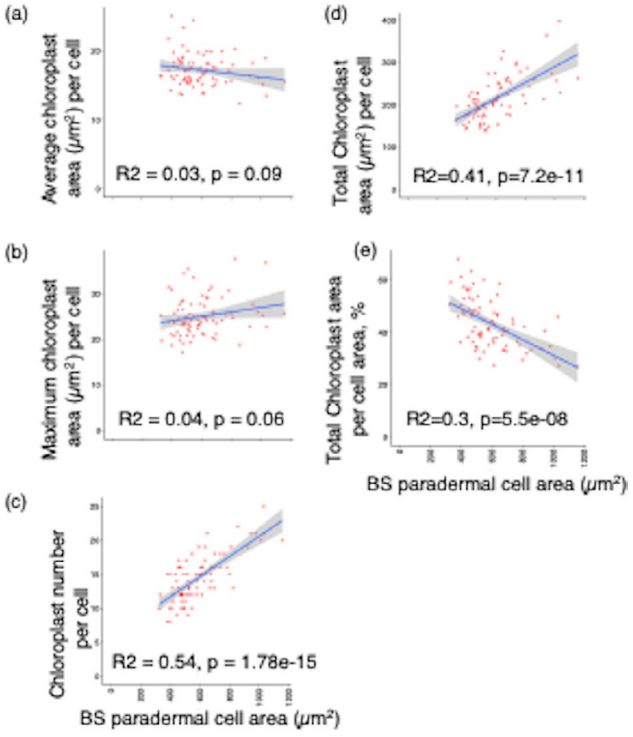

Fig. 6 Linear regression analysis between bundle sheath chloroplast parameters and paradermal cell area of wild-type rice. Linear regression plots representing bundle sheath (BS) paradermal cell area versus average chloroplast area (**a**), maximum chloroplast area (**b**), chloroplast numbers (**c**), total chloroplast occupancy (**d**), and relative chloroplast area in the cell (%). Graphs show the line of best fit and standard error (grey filled region) of the linear model fitted to the data (red circles)

been challenging to phenotype bundle sheath tissue in C_3 species as these cells are deeper in the leaf because of the many layers of mesophyll cells [27]. Approaches including bright-field light microscopy [18], transmission electron microscopy [23], serial block-face scanning electron microscopy [26] and single-cell isolation methods [22] are slow and so this hinders rapid analysis of transgenic lines harbouring candidate genes that are hypothesized to control chloroplast proliferation in the bundle sheath. To this end, we sought to establish a rapid and robust method to visualize bundle sheath cell files in C_3 rice.

Including sample preparation time, the ablation method reported here requires about 30 min to phenotype one leaf sample and can capture images from 30 to 40 bundle sheath cells in one focal plane. To obtain three-dimensional imaging via acquisition of z-stacks approximately one hour is needed. This compares favourably with other approaches such as the published single-cell isolation method [22] which involves five hours of sample preparation followed by three-four hours to image a similar number of cells. Thus, we estimate that the leaf ablation method is at least ten times faster than single-cell isolation. Other methods that involve resin-embedding, thin-sectioning, and then image capture via light or electron microscopy take a few weeks. The leaf ablation method also excludes hazardous chemicals and enzymes for sample preparation, and it is noteworthy that it also allows specific vein types to be identified prior to imaging, which can be challenging with the single-cell isolation method as the leaf tissue is subject to enzymatic digestion. We therefore consider this simple ablation approach to be robust and useful for high-throughput in vivo phenotyping of bundle sheath cells in C_3 species.

To provide evidence that imaging after ablation captures parameters derived from intact bundle sheath cells, the width of rice bundle sheath cells was measured from transverse sections obtained from serial block-face scanning electron microscopy (Additional file 2a) and compared with paradermal cell width obtained from confocal microscopy imaging after leaf ablation (Additional file 2b). As bundle sheath cells are cylindrical in rice [14], the width should equal the depth. In fact, mean bundle sheath cell width was lower (~10 µm) when estimated from transverse sections compared with paradermal sections (~15 µm; Additional file 2b) implying that the estimates of cell width after ablation are not associated with incomplete imaging of this cell type. It is also possible that paradermal sections preferentially captured information on bundle sheath cells lateral to each vein (Fig. 3a). It has been reported that during the C_3 to C_4 trajectory bundle sheath cells elongate less along the axis of the vein but become wider [14, 15]. Consistent with this, we observed a two-fold increase in bundle sheath cell width in maize compared with rice (Fig. 3c). However, the length of bundle sheath cells in the two species were similar and so these data suggest that a reduction in bundle sheath cell length may not be required for the evolution of C_4 photosynthesis. The average bundle sheath cell length in maize is similar to what has been previously reported [14]. However, they reported higher values for average rice bundle sheath cell length (~50 µm), compared to our study (~40 µm), which might be due to different growth conditions.

Under the conditions we used the average planar area of bundle sheath chloroplasts in wild-type and p*ZmUbi*::*ZmG2* was higher than in previous analysis [22]. These differences might result from different experimental conditions such as light intensity and/or from the use of confocal laser microscopy to study chloroplasts in our study. For example, Wang et al., 2017 used the single-cell isolation method followed by bright-field light microscopy. There is a possibility that chloroplast area is over-estimated from chlorophyll autofluorescence due to the introduction of background pixels. To investigate this, we measured the planar area of 574 bundle sheath chloroplasts from the two-dimensional images of wild-type rice leaf samples obtained from serial block-face scanning electron microscopy (Additional file 3a). Based on

this approach, the average area of individual chloroplasts was 14 μm^2 (Additional file 3b), which is higher than previously reported (11 μm^2; [22]) but lower than what we estimated from confocal imaging after ablation (16–17 μm^2; Figs. 4b and 5c). The reduction in bundle cell width and chloroplast area from serial block-face scanning electron microscopy compared with confocal imaging data might be due to tissue shrinkage during sample preparation [31, 32]. Thus, it implies that the larger chloroplast area might result from our experimental conditions than confocal imaging. Irrespective of these differences, leaf ablation in association with confocal imaging allows differences between genotypes to be detected (Fig. 4b, d). Although, we measured only planar chloroplast area, rice chloroplasts are often lobed [33, 34] and so in the future being able to estimate volume and surface area will help refine our understanding of the relationship between photosynthesis activity and leaf anatomy.

Conclusions

In conclusion, we report a simple and scalable leaf ablation method to access bundle sheath cell files in C_3 species such as rice. We show that this method is appropriate to measure bundle sheath cell dimensions, chloroplast areas and chloroplast numbers per cell. We also show bundle sheath cells are intact after the leaf ablation. As the approach is at least ten times faster than the next most efficient approach, ablation should significantly accelerate analysis of transgenic lines harbouring candidate genes aimed at modifying the rice bundle sheath.

Materials and methods

Plant material and growth conditions

Seeds of wild-type (*Oryza sativa spp japonica* cv. Kitaake) and maize *GOLDEN-2* (*ZmG2*) overexpressing rice ([22]; $ZmUBI_{pro}$::*ZmG2* line E131) were imbibed in sterile Milli-Q water and incubated at 30 °C in the dark for two days. Seeds were transferred onto Petri plates with moistened Whatman filter paper and germinated in the growth cabinet at 28 °C with 16/8 hrs. of light/dark cycle. After two days, germinated seedlings were potted into 9 by 9 cm pots (two plants/pot) filled with Profile Field and Fairway soil amendment (www.rigbytaylor.com). Plants were grown in a walk-in plant growth chamber under a 12-hour photoperiod at a photon flux density of 400 $\mu mol\ m^{-2}\ s^{-1}$ at 28°c (day) and 20 °C night. Once a week, plants were fed with the Peters Excel Cal-Mag Grower fertiliser solution (LBS Horticulture, Clone, UK) with additionally supplied iron (Fe7 EDDHA regular, Gardening Direct, UK). The working fertiliser solution contains 0.33 g/L of Peters Excel Cal-Mag Grower and 0.065 g/L chelated iron. Maize (B73) seeds were germinated on wet filter paper in the dark at 28 °C for three days after which each germinated seed was transferred into a two litre pot containing a mixture of two parts nutrient-rich compost (Levington Advance M3, ICL, Ipswich, UK) to one part topsoil (Westland, Dungannon, Northern Ireland), 10 ml Miracle-Gro all-purpose fertiliser beads and 15 ml Miracle-Gro magnesium salt (Scotts Miracle-Gro, Marysville, OH, USA). They were grown in a growth cabinet operating at 28 °C (day)/ 20 °C (night) at a photon flux density of 550 $\mu mol\ m^{-2}\ s^{-1}$ under a 14-hour photoperiod.

Sample preparation

The middle region of the fully expanded fourth leaf from wild-type Kitaake, $ZmUBI_{pro}$::*ZmG2* overexpressing rice lines and maize was fixed with 1% (w/v) glutaraldehyde in 1X PBS buffer. Once fixative was infiltrated, samples were left in that solution for about two hours and then washed twice with 1X PBS buffer, with each wash lasting ~ 30 min. Leaf samples can be stored in 1X PBS buffer at 4 °C for several weeks without losing chlorophyll autofluorescence. Before microscopy, the adaxial side of the fixed leaf material was ablated gently with a fine razor blade (Personna, Verona, VA 24,482; Additional file 1) to remove mesophyll layers. This process requires two to three minutes to scrape off the epidermis and mesophyll tissue to expose rice bundle sheath cells surrounding intermediate veins (Additional file 1). As maize contains fewer mesophyll layers, it took less than a minute to ablate mesophyll layers. Bundle sheath cells can be directly visualized with light microscopy. For confocal microscopy, the ablated leaf fragment was stained with the cell wall stain calcofluor white (0.1%; Sigma) for 5 min and then rinsed twice with H_2O.

Light and confocal laser microscopy

Light microscopy images (Olympus BX51 microscope) of both rice and maize leaves were captured using an MP3.3-RTV-R-CLR-10-C MicroPublisher camera and QCapture Pro 7 software (Teledyne Photometrics, Birmingham, UK) to visualize the differences before and after the ablation. A Leica SP8X confocal microscope upright system (Leica Microsystems) was used for fluorescence imaging. It has two continuous wave laser lines, 405 and 442 nm, a 460–670 nm super continuum white light laser (WLL) and four hybrid detectors and one photomultiplier tube. Imaging was conducted using a 25X water immersion objective and Leica Application Suite X (LAS X; version: 3.5.7.23225) software. Calcofluor white was excited at 405 nm and emitted fluorescence captured from 452 to 472 nm. Chlorophyll autofluorescence was excited at 488 nm and emission captured 672–692 nm. Three replicates from both wild-type Kitaake and $ZmUBI_{pro}$::*ZmG2* overexpression line E131 were analysed. Z-stacks of ~ 30 lateral bundle sheath cells surrounding three different intermediate veins (3°) and eight to ten cells per vein were obtained from each replicate. From three replicates,

82 and 90 bundle sheath cells from wild-type and E131 line were imaged respectively. Maximum intensity projection images were used to quantify bundle sheath cell dimensions, individual chloroplast areas and chloroplast number per cells. Bundle sheath cell length and width were measured at the mid-point of the proximal-distal and medio-lateral axes respectively. Images of 90 maize bundle sheath cells of intermediate veins from three replicates were captured using confocal laser microscopy to measure bundle sheath cell dimensions.

Serial block-face scanning electron microscopy

Wild-type rice leaf (middle region of fourth leaves) samples were fixed in fixative (2% w/v glutaraldehyde / 2% w/v formaldehyde in 0.05 M sodium cacodylate buffer pH 7.4 containing 2 mM calcium chloride) overnight at 4°C. After washing five times with 0.05 M sodium cacodylate buffer pH 7.4, samples were osmicated (1% osmium tetroxide, 1.5% potassium ferricyanide, 0.05 M sodium cacodylate buffer pH 7.4) for three days at 4°C. After washing five times in DIW (deionised water) samples were treated with 0.1% (w/v) thiocarbohydrazide/DIW for 20 min at room temperature in the dark. After washing five times in DIW, samples were osmicated a second time for one hour at RT (2% osmium tetroxide/DIW). After washing five times in DIW, samples were block stained with uranyl acetate (2% uranyl acetate in 0.05 M maleate buffer pH 5.5) for three days at 4°C. Samples were washed five times in DIW and then dehydrated in a graded series of ethanol (50%/70%/95%/100%/100% dry), 100% dry acetone and 100% dry acetonitrile, three times in each for at least five minutes. Samples were infiltrated with a 50/50 mixture of 100% dry acetonitrile/Quetol resin mix (without BDMA) overnight, followed by three days in 100% Quetol (without BDMA). Then, the sample was infiltrated for five days in 100% Quetol resin with BDMA, exchanging the resin each day. The Quetol resin mixture is: 12 g Quetol 651, 15.7 g NSA (nonenyl succinic anhydride), 5.7 g MNA (methyl nadic anhydride) and 0.5 g BDMA (benzyldimethylamine; all from TAAB). Samples were placed in embedding moulds and cured at 60°C for three days.

Sections were cut at a thickness of about 70 nm using a Leica Ultracut E, placed on a Melinex plastic coverslip, and allowed to air dry. Coverslips were mounted on aluminium scanning electron microscopy stubs using conductive carbon tabs and the edges of the slides were painted with conductive silver paint. Then, samples were sputter coated with 30 nm carbon using a Quorum Q150 TE carbon coater. Samples were imaged in a Verios 460 scanning electron microscope (FEI/Thermofisher) at 4 keV accelerating voltage and 0.2 nA probe current in backscatter mode using the concentric backscatter detector (CBS) in field-free mode for low magnification imaging and in immersion mode at a working distance of 3.5-4 mm; 1536×1024 pixel resolution, 3 us dwell time, 4 line integrations for higher magnification imaging. Stitched maps were acquired using FEI MAPS automated acquisition software using the default stitching profile and 5% image overlap. Transverse bundle sheath cell width was measured from bundle sheath cells of three minor veins per replicate, and three biological replicates were used. In total, dimensions of 92 bundle sheath cells were measured. The planar chloroplast areas were measured from paradermal sections of bundle sheath cells surrounding two minor veins per replicate. Total areas of 574 chloroplasts were measured across 130 cells.

Data analyses

Bundle sheath cell dimensions (length, width, and area), chloroplast area and numbers per cell were measured using ImageJ version 2.1.0/1.53c [35]. RStudio (version:1.4.1106) was used to plot the data using the ggplot2 software package [36] and statistical analysis was performed using the ggpubr software package [37]. First, equality of variance between the two groups was tested using Barlett's test [38]. Where the assumption of equal variance was met, a two-tailed pairwise t-test (Student's t-test) was performed. Otherwise, Welch's two-sample t-test was performed. A general linear regression model was performed using the ggfortify package [39] and assumptions of a linear regression model were tested using the autoplot function of the ggfortify package. Finally, the general linear regression line was fitted using the lm function and, ANOVA test was performed to test whether the slope is significantly different from zero.

Supplementary Information

The online version contains supplementary material available at https://doi.org/10.1186/s13007-023-01041-x.

Additional file 1: Movie showing rice leaf ablation. Rice leaf image with different vein orders before and after leaf ablation (top) and video showing the leaf ablation process (bottom). A drop of water was added onto a glass plate to prevent the dehydration while ablating the leaf. 1°: primary/mid vein; 2°: secondary/large lateral veins; 3°: tertiary/intermediate veins. Movie courtesy: Dr Satish Kumar Eeda. **Additional file 2**: Comparison of bundle cell width in paradermal versus transverse sections obtained from confocal laser scanning microscopy versus serial block-face scanning electron microscopy (SBF-SEM), respectively. (**a**) Transverse section of a rice leaf obtained from serial block-face scanning electron microscopy, representing the bundle sheath cells of a tertiary vein (3°). Bundle sheath cell width was measured at the mid-point of the medio-lateral axes as annotated with a red arrow. (**b**) Comparison of bundle sheath cell width measurements from paradermal and transverse sections, obtained from confocal imaging (rice data from Fig. 3c) and serial block-face scanning electron microscopy, respectively. BS: Bundle sheath cell; M: Mesophyll cell. Blue dot in the violin plots represent mean values. Statistical test: t-test. **Additional file 3**: Comparison of individual chloroplast areas obtained from confocal laser scanning microscopy versus serial block-face scanning electron microscopy (SBF-SEM). (**a**) Paradermal section of a rice leaf obtained from serial block-face scanning electron microscopy, representing the lateral bundle sheath cells of a tertiary vein (3°). Bundle sheath chloroplasts were pointed with red arrows. (**b**) Comparison of individual chloroplast areas

from confocal (wild-type rice data from Fig. 4b) and two-dimensional serial block-face scanning electron microscopy imaging. BS: Bundle sheath cell; M: Mesophyll cell. Blue dot in the violin plots represent mean values. Statistical test: t-test.

Acknowledgements
This research was funded by a C_4 Rice Project grant (#INV-002970) from The Bill & Melinda Gates Foundation to the University of Oxford. For the purposes of open access, the authors have applied a Creative Commons Attribution (CC BY) license to any Author Accepted Manuscript version arising from this submission. We thank Dr Lei Hua for useful suggestions for confocal laser microscopy work, Dr Lee Cackett for providing maize leaf material and Dr Tina B. Schreier for her guidance on serial block-face scanning electron microscopy work. We also thank Prof. Jane Langdale for providing rice seeds of *ZmUBI*$_{pro}$::*ZmG2* overexpressing line. We thank Dr Karin H Müller and Georgina E Lindop from the Cambridge Advanced Imaging Centre (CAIC) for the electron microscopy sample preparation as well as image acquisition.

Author contributions
KB designed and performed the experiments. KB drafted the manuscript. KB and JMH reviewed and edited the manuscript.

Data Availability
All data supporting the findings of this study are available within the paper and within its supporting information data published online.

Declarations

Ethics approval and consent to participate
.
Not applicable.

Consent for publication
Not applicable.

Competing interests
The authors declare no competing interests.

Received: 31 March 2023 / Accepted: 19 June 2023
Published online: 06 July 2023

References

1. Calvin M, Benson AA. The path of Carbon in Photosynthesis. Science. 1948;107:476–80.
2. Benson AA, Calvin M. Carbon dioxide fixation by green plants. Annu Rev Plant physiol. 1950;1:25–42.
3. Edwards GE, Walker DA. C3, C4:mechanisms, and cellular and environmental regulation, of photosynthesis. Oxford, UK: Blackwell Sci; 1983.
4. Ehleringer JR, Sage RF, Flanagan LB, Pearcy RW. Climate change and the evolution of C4 photosynthesis. Trends in Ecology and Evolution. 1991;6:95–9.
5. Borland AM, Zambrano VAB, Ceusters J, Shorrock K, Zambrano VAB, Ceusters J, et al. The photosynthetic plasticity of crassulacean acid metabolism: an evolutionary innovation for sustainable productivity in a changing world. New Phytol. 2011;191:619–33.
6. Sage RF, Stata M. Photosynthetic diversity meets biodiversity: the C4 plant example. J Plant Physiol. 2015;172:104–19.
7. Hatch MD. C4 photosynthesis: a unique blend of modified biochemistry, anatomy and ultrastructure. Biochimica et Biophysica Acta (BBA) - reviews on Bioenergetics. 1987;895:81–106.
8. Ehleringer JR, Monson RK. Evolutionary and ecological aspects of photosynthetic pathway variation. Annu Rev Ecol Syst. 1993;24:411–39.
9. Sage RF, Pearcy RW. The Nitrogen Use Efficiency of C3 and C4 plants. Plant Physiol. 1987;85:355–9.
10. Zhu X-G, Long SP, Ort DR. Improving photosynthetic efficiency for greater yield. Annu Rev Plant Biol. 2010;61:235–61.
11. Sage RF, Zhu X-G. Exploiting the engine of C4 photosynthesis. J Exp Bot. 2011;62:2989–3000.
12. Edwards GE, Voznesenskaya EV. In: Raghavendra AS, Sage RF, editors. C4 photosynthesis: Kranz Forms and single-cell C4 in terrestrial plants. Dordrecht: Springer Netherlands; 2011. pp. 29–61. http://link.springer.com/. https://doi.org/10.1007/978-90-481-9407-0_4.
13. Haberlandt G. Physiologische Pflanzenanatomie, Leipzig, Germany: Verlag von Wilhelm Engelmann. Verlag von Wilhelm Engelmann; 1904.
14. Danila FR, Quick WP, White RG, Kelly S, von Caemmerer S, Furbank RT. Multiple mechanisms for enhanced plasmodesmata density in disparate subtypes of C4 grasses. J Exp Bot. 2018;69:1135–45.
15. Khoshravesh R, Stata M, Busch FA, Saladié M, Castelli JM, Dakin N, et al. The evolutionary origin of C4 photosynthesis in the grass subtribe neurachninae. Plant Physiol. 2020;182:566–83.
16. Sage RF, Khoshravesh R, Sage TL. From proto-kranz to C4 Kranz: building the bridge to C4 photosynthesis. J Exp Bot. 2014;65:3341–56.
17. Hibberd JM, Sheehy JE, Langdale JA. Using C4 photosynthesis to increase the yield of rice-rationale and feasibility. Curr Opin Plant Biol. 2008;11:228–31.
18. Khoshravesh R, Stinson CR, Stata M, Busch FA, Sage RF, Ludwig M, et al. C3-C4 intermediacy in grasses: organelle enrichment and distribution, glycine decarboxylase expression, and the rise of C2 photosynthesis. J Exp Bot. 2016;67:3065–78.
19. Langdale JA, Kidner CA, Langdale JA, Kidner CA. Bundle sheath defective, a mutation that disrupts cellular differentiation in maize leaves. Development. 1994;120:673–81.
20. Hall LN, Rossini L, Cribb L, Langdale JA. GOLDEN 2: a novel transcriptional regulator of cellular differentiation in the maize leaf. Plant Cell. 1998;10:925–36.
21. Lambret-Frotte J, Smith G, Langdale JA. GOLDEN2-like1 is sufficient but not necessary for chloroplast biogenesis in mesophyll cells of C4 grasses [Internet]. bioRxiv; 2023. https://www.biorxiv.org/content/https://doi.org/10.1101/2023.02.10.528040v1.
22. Wang P, Khoshravesh R, Karki S, Furbank R, Sage TL, Langdale JA, et al. Re-creation of a key step in the Evolutionary switch from C3 to C4 Leaf anatomy. Curr Biol. 2017;27:3278–3287e6.
23. Stata M, Sage TL, Hoffmann N, Covshoff S, Wong GK-S, Sage RF. Mesophyll chloroplast investment in C3, C4 and C2 species of the genus Flaveria. Plant Cell Physiol. 2016;57:904–18.
24. Romanowska E, Parys E. Mechanical isolation of bundle sheath cell strands and thylakoids from leaves of C4 grasses. Methods Mol Biol. 2011;684:327–37.
25. Kanai R, Edwards GE. Separation of mesophyll protoplasts and bundle sheath cells from maize leaves for photosynthetic studies. Plant Physiol. 1973;51:1133–7.
26. Harwood R, Goodman E, Gudmundsdottir M, Huynh M, Musulin Q, Song M, et al. Cell and chloroplast anatomical features are poorly estimated from 2D cross-sections. New Phytol. 2020;225:2567–78.
27. Griffiths H, Weller G, Toy LFM, Dennis RJ. You're so vein: bundle sheath physiology, phylogeny and evolution in C3 and C4 plants. Plant Cell Environ. 2013;36:249–61.
28. Sedelnikova OV, Hughes TE, Langdale JA. Understanding the genetic basis of C4 Kranz anatomy with a view to Engineering C3 crops. Annu Rev Genet. 2018;52:249–70.
29. Long SP, Zhu X-GG, Naidu SL, Ort DR. Can improvement in photosynthesis increase crop yields? Plant. Cell and Environment. 2006;29:315–30.
30. von Caemmerer S, Quick WP, Furbank RT. The development of C_4 rice: current progress and future challenges. Science. 2012;336:1671–2.
31. Talbot MJ, White RG. Cell surface and cell outline imaging in plant tissues using the backscattered electron detector in a variable pressure scanning electron microscope. Plant Methods. 2013;9:40.
32. Lee M-S, Boyd RA, Boateng KA, Ort DR. Exploring 3D leaf anatomical traits for C4 photosynthesis: chloroplast and plasmodesmata pit field size in maize and sugarcane. New Phytologist. 2023.
33. Ouk R, Oi T, Sugiura D, Taniguchi M. 3-D reconstruction of rice leaf tissue for proper estimation of surface area of mesophyll cells and chloroplasts facing intercellular airspaces from 2-D section images. Ann Botany. 2022;130:991–8.
34. Oi T, Enomoto S, Nakao T, Arai S, Yamane K, Taniguchi M. Three-dimensional intracellular structure of a whole rice mesophyll cell observed with FIB-SEM. Ann Botany. 2017;120:21–8.
35. Schneider CA, Rasband WS, Eliceiri KW, Instrumentation C. NIH Image to ImageJ: 25 years of image analysis. Nat Methods. 2012;9:671–5.
36. Wickham H. ggplot2: Elegant Graphics for Data Analysis [Internet]. Springer, New York; 2009. p. 65–90. https://link.springer.com/https://doi.org/10.1007/978-0-387-98141-3.
37. Kassambara A, ggpubr. "ggplot2" Based Publication Ready Plots. 2023. https://CRAN.R-project.org/package=ggpubr.

38. Bartlett MS. Properties of Sufficiency and statistical tests. In: Kotz S, Johnson NL, editors. Breakthroughs in statistics [Internet]. New York, NY: Springer; 1992. pp. 113–26. https://doi.org/10.1007/978-1-4612-0919-5_8.
39. Tang Y, Horikoshi M, Li W. ggfortify: Unified Interface to visualize statistical results of Popular R Packages. R J. 2016;8:474.

Publisher's Note